COVARIANCE PROPAGATION WITH TIME-CORRELATED ERRORS

Alejandro Cano[(1)], **Manuel Sanjurjo-Rivo**[(1)], **Joaquín Míguez**[(1)], **Alejandro Pastor**[(2)], **and Diego Escobar**[(2)]

[(1)]*Universidad Carlos III de Madrid, Avenida Universidad 30, Leganés 28911, Spain. Email: [alejandro.cano@alumnos.uc3m.es, alcano@gmv.com], joaquin.miguez@uc3m.es, manuel.sanjurjo@uc3m.es*
[(2)]*GMV, Calle Isaac Newton 11, Tres Cantos, 28670, Spain. Email: apastor@gmv.com, descobar@gmv.com*

ABSTRACT

The space objects population is expected to continue its rapid growth due to many factors such as the mega-constellations and a wider accessibility to the space, but also from fragmentation events whose occurrences are increasing. In such situation, Space Situational Awareness (SSA) services and products are of the utmost relevance to maintain the safety and sustainability of the spacecraft operations. Most SSA products rely in the knowledge of both the state of the Resident Space Object (RSO) and its associated uncertainty, or in other words, the Probability Density Function (PDF) that describes the state of the object. For many SSA products such as collision risk analysis or catalogue maintenance, the uncertainty of the state is represented as a covariance matrix, retaining only up to the second order moment of the state PDF. This choice is generally based on a trade-off between accuracy and computational efficiency. Under this assumption, it is necessary to consider the different sources of uncertainty that are present in the space environment in order to improve the covariance realism. For these reasons, it is necessary to develop efficient and accurate methodologies to characterise the PDF of the state attending to the different sources of uncertainty, which is known as Uncertainty Quantification (UQ).

In this work, we present a covariance propagation methodology named as Linear Stochastic Parameters (LSP), based on linear theory that allows to analyze the effect of time-correlated errors on the covariance evolution. Linear covariance propagation theory can consider the impact of the uncertainty of dynamical parameters on the evolution of the state by means of the so-called sensitivity matrix, resulting from the integration of the variational equations, and the consider parameter theory. However, the correlation between parameters is not generally considered during linear propagation. In that line, we present here a method to compute efficiently the effect of a series of uncertain time-correlated parameters on the covariance. First, an auto-regressive function of order 1 AR(1) is used to model the time correlation in the sequence of parameters, controlling the correlation strength by means of the power of the noise and the time-scale of the correlation. Second, the properties of the variational equations are exploited in order to compute the sensitivity matrix, in this case, of a series of multiple uncertain parameters of the same kind (e.g. atmospheric drag errors) from the case where a single constant uncertain parameter is considered. This formulation allows to analyse the impact of stochastic perturbations on the covariance evolution without requiring the integration of stochastic equations of motion, and allowing to derive different perturbation models ranging from Gaussian noise up to a constant perturbation depending on the selected correlation time-scale. In this work, the LSP method is described and applied to model the stochastic atmopsheric density, represented with an AR(1) function. The methodology is validated via Monte Carlo simulations with stochastic dynamics, focusing on the achievable accuracy and computational time performance.

Keywords: Covariance propagation; time-correlation; atmospheric density uncertainty, stochastic dynamics.

1. INTRODUCTION

In the currently overcrowded space environment, Space Situational Awareness (SSA) and Space Traffic Management (STM) services become the cornerstone for the sustainability and efficiency of the space operations. SSA deals with the capability of detecting, predicting and assessing any hazard towards the active spacecraft population orbiting the Earth, providing products such as collision risk assessment, re-entry prediction or fragmentation analysis, among others. In order to provide such services, Earth-orbiting objects (active or not, including debris) are routinely tracked to estimate and predict their state (i.e. position, velocity, and dynamic parameters). However, the quality of these products does not only rely on the estimation and prediction of the state, but also in the proper characterisation of the complete Probability Distribution Function (PDF) defining the state uncertainty. The estimation and prediction of such uncertainty is a wide field of study generally known as Uncertainty Quantification (UQ). The uncertainty of the state is represented as a PDF due to the many sources of uncertainty present, for instance, due to the accuracy of the observations or the limited knowledge of the dynamical system [18][10].

Proc. 2nd NEO and Debris Detection Conference, Darmstadt, Germany, 24-26 January 2023, published by the ESA Space Safety Programme Office
Ed. T. Flohrer, R. Moissl, F. Schmitz (http://conference.sdo.esoc.esa.int, February 2023)

SSA activities suffer from data scarcity, this is, that the availability of observations for the Resident Space Objects (RSO) is very sparse due to having on-collaborative objects as targets (debris) and limited network capacities, which has a significant impact on the orbit estimation processes. Therefore, the prediction of the state and its uncertainty is key for accurate tracking and services reliability, typically known as Uncertainty Propagation (UP). Methods and classifications for UP have been extensively studied in the literature [13][1].

Among the wide variety of complexities, efficiency and applications of the different methods, a trade-off is generally made between complexity against accuracy when propagating the initial PDF of the state. Some methodologies pledge for simplicity and efficiency, at the expense of accuracy and, on many occasions, applying simplifications such as representing the PDF of the state with only the two first moments of the distribution, i.e. the mean and covariance. Some examples of these cases are linear propagation via State Transition Matrix (STM) [16] or Kalman Filters and their variants [24]. Though simple, fast, and accurate depending on the system conditions, their main drawback is that the linear approximation of the dynamics deteriorates with increasing propagation intervals and growing initial uncertainty volumes, as well as in the presence of agents that accelerate the development of non-linearities in the dynamics such as the atmospheric drag.

Several complex implementations that do not rely on the linearization of the dynamics are widely studied nowadays, such as the Unscented Transform (UT) and Cubature methods [12][7], Polynomial Chaos Expansions (PCE) [27][11], Differential Algebra (DA) [4][3], State Transition Tensors (STT) [17], Gaussian mixtures [2][8][26], Particle Filters [14][15] or the well-known Monte Carlo methods.

Nonetheless, nominal spacecraft operators require simple but effective methods to propagate the uncertainty of the state, generally assuming hypothesis such as Gaussianity and linearity. Therefore, it is relevant to develop methodologies that, even under the previous assumptions, are able to represent the uncertainty sources of the space environment. In LEO objects, the atmospheric drag is one of the most perturbing forces, and the lack of knowledge on the objects characteristics or the aleatory nature of the atmosphere causes the drag uncertainty to be one of the most relevant and studied sources of uncertainty. The complex modelling of the atmospheric density and its dependence on space weather parameters such as the Solar Flux or Geomagnetic indexes lead to differences of around 20% even between most modern models of the atmosphere [25].

For all these reasons, stochastic processes have been extensively applied to model the aleatory behavior of atmospheric density. White noise and Brownian motion have been proposed to model the stochastic nature of the Solar Flux [21][9]. Other studies propose more complex noise models, based on white noise but with a controlled tendency to mean values, such as Ornstein-Uhlenbeck [20]. Moreover, stochastic models that include time or spatial noise correlation are an extensive line of analysis. Gauss-Markov models, which can be defined as a special case of an Ornstein-Uhlenbeck process, include different time correlation scales. In [22], improvements in covariance realism were observed when applying a Gauss-Markov stochastic model in Kalman filter estimation as compared with batch estimation. Nonetheless, despite the many studies with the aforementioned stochastic density models for the atmosphere, operational applications of such noise models are not common since, as previously mentioned, most operational applications still rely on linear propagation, while other simple but accurate approaches such as Monte Carlo are high time consuming.

In this work, we present a novel method, named as Linear Stochastic Parameter (LSP) covariance propagation, that allows to analyse the effect of stochastic time-correlated uncertainty on the time evolution of the covariance, avoiding the integration of stochastic equations of motion. The method is based on linear propagation theory and exploits the properties of the variational equations to derive an efficient, yet accurate, procedure to characterize stochastic noise sequences. The basis of the methodology is to conceptually subdivide any uncertain parameter (i.e. drag coefficient), typically applied throughout the whole propagation arc, into multiple parameters. However, each of those parameters are now defined as members of the stochastic noise sequence, modelled by an auto-regressive function of order 1 AR(1). Then, a procedure to model the effect of the noise sequence as a linear product for the linear covariance propagation is defined. The LSP method is applicable to any uncertain parameter such as the drag coefficient, the solar radiation pressure coefficient or even manoeuvre modulus or direction uncertainty.

The work presented here serves as a first validation approach for this methodology. The atmospheric density uncertainty is modelled with the AR(1) stochastic dynamics, being dependent on an expected uncertainty of the atmosphere each position, and controlled by a time scale parameter. Monte Carlo (MC) simulations with Stochastic Differential Equations (SDE) are conducted for the validation of the LSP covariance propagation method, focusing on the achievable accuracy and computational time improvement. The reminder of the work is structured as follows. Section 2 presents the LSP methodology. Section 3 describes the validation process and shows the most relevant validation results. Once validated, Section 4 provides further discussion on LSP methodology results and execution time performance. Finally, Section 5 contains the most relevant conclusions of the work and future lines of improvement.

2. METHODOLOGY

This section describes the theoretical development of the LSP covariance propagation method. Firstly, the linear propagation method of the covariance is revisited. Secondly, the stochastic drag force model and the atmospheric correlated noise is detailed. Finally, the procedure to consider such correlated noise into the linear covariance propagation is explained.

2.1. Linear covariance propagation

A complete derivation of linear propagation theory can be found in many well-known references, such as [16]. First, let us define the extended state vector as

$$\mathbf{y_{ext}} = \begin{pmatrix} \mathbf{r}(t) \\ \mathbf{v}(t) \\ \mathbf{q}(t) \\ \mathbf{c}(t) \end{pmatrix} \in \mathbb{R}^{n_x+n_q+n_c} \tag{1}$$

which is composed of the state vector $\mathbf{x}(t) = (\mathbf{r}(t), \mathbf{v}(t))$ of size n_x, estimated parameters **q(t)** of size n_q and the consider (uncertain) parameters of our analysis **c(t)**, of size n_c. To account for the effect of the main dynamic parameters in the propagation of the state, it is required to integrate the variational equations. Its solution is the Extended State Transition Matrix (ESTM)

$$\begin{gathered} \mathbf{\Psi}\left(t, t_0\right) = \begin{pmatrix} \mathbf{\Phi}\left(t, t_0\right) & \mathbf{S}\left(t, t_0\right) \\ \mathbf{0} & \mathbf{I} \end{pmatrix} \\ \mathbf{\Psi} \in \mathbb{R}^{(n_x+n_p)\times(n_x+n_p)} \\ \mathbf{\Phi} \in \mathbb{R}^{6\times 6} \\ \mathbf{S} \in \mathbb{R}^{6\times n_p} \\ \mathbf{I} \in \mathbb{R}^{n_p\times n_p} \end{gathered} \tag{2}$$

where:

- n_p is the number of dynamical parameters to consider during propagation, which in this case corresponds to the estimated dynamical parameters plus the consider parameters, excluding position and velocity: $n_p = n_q + n_c$
- $\mathbf{\Phi}\left(t, t_0\right)$ corresponds to the state transition matrix, which relates the position and velocity at any time t with respect to the initial state at time t_0.
- $\mathbf{S}\left(t, t_0\right)$ is the so-called sensitivity matrix, which contains the partial derivatives of the state vector with respect to the model dynamical parameters, both estimated and considered. These parameters are normally defined as constant in the dynamic model as is customary in many propagation methods [23]. The uncertainty of these constant parameters is mapped into the state covariance by means of the sensitivity matrix.

The ESTM can be computed by solving numerically its associated partial differential equations as shown in [16]. To account for the effect of the uncertainty of the consider parameters in our covariance propagation, we have

$$\begin{gathered} \mathbf{P}(t) = \mathbf{\Psi}\left(t, t_0\right) \mathbf{P}\left(t_0\right) \mathbf{\Psi}\left(t, t_0\right)^T = \\ = \begin{pmatrix} \mathbf{\Phi}\left(t, t_0\right) & \mathbf{S}\left(t\right) \\ \mathbf{0} & \mathbf{I} \end{pmatrix} \begin{pmatrix} \mathbf{P}_0 & \mathbf{0} \\ \mathbf{0} & \mathbf{C} \end{pmatrix} \mathbf{\Psi}\left(t, t_0\right)^T \\ \text{with } \mathbf{P}(t) \in \mathbb{R}^{(n_x+n_p)\times(n_x+n_p)} \end{gathered} \tag{3}$$

where $\mathbf{P}_0$ is the initial state covariance, and $\mathbf{C}$ contains the uncertainty of the parameters. Such consider parameters are typically defined as constant in the linear formulation, with a certain variance, for the complete propagation or determination arcs.

2.2. Drag force with correlated noise

Let us describe now the stochastic drag force model to be applied in the system dynamics, detailing the time-correlated noise model for the atmospheric density. The classical definition of the drag force acceleration is

$$\boldsymbol{a}_{\text{drag}}\left(t\right) = -\frac{1}{2}\rho(t)\frac{C_D A}{m} v_{rel}(t)^2 \frac{\boldsymbol{v}_{rel}(t)}{\left|\boldsymbol{v}_{\text{rel}}\left(t\right)\right|} \tag{4}$$

where C_D the drag coefficient, A the cross-sectional area, m the object mass, v_{rel} is the relative speed of the object with respect to the atmosphere and $\rho(t)$ is the atmospheric density. The ballistic coefficient term ($C_D A/m$) (i.e. the ballistic coefficient) is normally obtained as part of the OD process. Though the cross-sectional area or the drag coefficient are known to vary along the trajectory of the object, the ballistic coefficient is considered to be constant in the propagation arcs considered in this work, as it is approximated in most SSA operational scenarios for non-collaborative objects. We model the stochastic atmospheric density as

$$\rho(t) = \bar{\rho}(t) + p(t) \tag{5}$$

where $p(t)$ represents the perturbing noise, and $\bar{\rho}(t)$ corresponds to the mean atmospheric density at a certain position and epoch, obtained with the NRLMSISE-00 model in this work. To introduce a zero-mean correlated noise sequence for the perturbation error, an autoregressive function with time correlation of order 1 AR(1) is proposed [5]. First, let us assume that the correlation of two perturbations at two consecutive time steps $p\left(t_n\right)$ and $p\left(t_{n-1}\right)$, in discrete form, is as

$$r_p\left(t_n, t_{n-1}\right) = \mathrm{E}\left[p\left(t_n\right) p\left(t_{n-1}\right)\right] = r_0\left(t_n\right) e^{-\alpha\left|t_n - t_{n-1}\right|} \tag{6}$$

where $r_0(t_n) = \mathrm{E}\left[p(t_n)^2\right]$ is the power of the non-stationary perturbation. Such correlation of Eq. 6 can be guaranteed with the AR(1) model, as

$$p(t_n) = a(n)p(t_{n-1}) + u(n), \tag{7}$$

with

$$a(n) = \frac{r_0(t_n)}{r_0(t_{n-1})} e^{-\alpha(t_n - t_{n-1})}, \tag{8}$$

$$u(n) \sim \mathrm{N}\left(0, \sigma_u^2(n)\right) \tag{9}$$

$$\sigma_u^2(n) = r_0(t_n)\left[1 - \frac{r_0(t_n)}{r_0(t_{n-1})} e^{-2\alpha(t_n - t_{n-1})}\right], \text{and} \tag{10}$$

$$p(t_0) = u(0) \sim \mathrm{N}(0, r_0(t_0)) \tag{11}$$

Thus, the noise at each step is related to the previous noise by a factor $a(n)$ and has a Gaussian term $u(n)$. The strength of the correlation is controlled by $\alpha = 1/\tau_\alpha$ $[1/s]$, which represents the inverse of the time scale of correlation. This scale determines the strength of the correlation. The variance of the Gaussian term, $\sigma_u^2(n)$, is also dependent on the power noise, but inversely proportional to the correlation. In other words, the stronger the correlation in the noise, the smaller the Gaussian term becomes.

Combining the noise model with the classical drag force, the stochastic model for the drag is

$$\boldsymbol{a}_{\text{drag}}(t) = -\frac{1}{2}\bar{\rho}(t)\frac{C_D A}{m} v_{rel}(t)^2 \frac{\boldsymbol{v}_{rel}(t)}{|\boldsymbol{v}_{\text{rel}}(t)|}(1 + z(t)) \tag{12}$$

Where $z(t) = p(t)/\bar{\rho}(t)$ is the non-dimensional stochastic noise. It can be noted from Equations 8 and 9 that two limiting cases appear. If we assume constant power noise ($r_0(t_n) = r_0(t_{n-1})$), in the limit when the correlation time scale tends to infinity ($\tau_\alpha \approx \infty$) we find

$$\sigma_u^2(n) = 0; p(t_n) = p(t_{n-1}). \tag{13}$$

Thus, the stochastic noise is reduced to a constant noise model. On the opposite side, when the correlation time scale tends to very small values ($\tau_\alpha \approx 0$) we end up with

$$\sigma_u^2(n) = r_0^2(t_n); a(n) = 0; p(t_n) = u(n). \tag{14}$$

This is, a purely Gaussian noise. These limits are relevant to understand the maximum and minimum impact that the stochastic noise can achieve in the covariance time evolution depending on the selected correlation time scale, which is a parameter analysed in this work. Finally, it remains to describe the power of the noise sequence $r_0(t_n)$. It is chosen as the expected variance of the atmosphere σ_{atm}^2, computed as a function of altitude, latitude and altitude. This uncertainty of the atmosphere can be a subject of more in depth studies, and it is not the objective of this work. To apply realistic values, the results of atmospheric density standard deviation, derived statistical analysis of historical space weather data [6][1], are used in this work.

2.3. Correlated parameters in linear covariance propagation

Once explained the noise correlation model, the objective now is to assess the impact during covariance propagation due to the correlation of a parameter, such as the previously described atmospheric density. However, as described in Section 2.1, linear propagation assumes any uncertain parameter to be constant and with a fixed variance. Therefore, the proposed approach is to divide such global parameter into multiple ones, applied sequentially in time, and correlated in time according stochastic model defined in Section 2.2.

In addition, linear covariance propagation generall the modelled uncertain parameters to follow a Normal distribution with null mean and a certain variance in order to assume. Therefore, we define $u(n)$ of Equation 7 as our uncertain parameters. It can be noted that Equation 7 can be written as a linear product in matrix form for the complete set of time steps as:

$$\mathbf{p} = \mathbf{A}\mathbf{u}, \tag{15}$$

where

$$\mathbf{p} = \begin{pmatrix} p_0 \\ \vdots \\ p_n \end{pmatrix}; \mathbf{u} = \begin{pmatrix} u_0 \\ \vdots \\ u_n \end{pmatrix}; \tag{16}$$

$$\mathbf{A} = \begin{pmatrix} 1 & \cdots & 0 \\ \vdots & \ddots & \vdots \\ a_{ij} & \cdots & 1 \end{pmatrix} \in \mathbb{R}^{N \times N}, \tag{17}$$

Where $N = n + 1$ is the number of stochastic parameters, which corresponds to the amount of time-steps in the noise sequence. Finally, $a_{ij} = \prod_1^i a(n);\ \forall\ i < j$, where i and j represent the row and column of the matrix, respectively.

Returning to the propagation of the covariance, the ESTM is composed of the state transition matrix and the sensitivity matrix. We need the latter to be referred to our uncertain parameter vector ($\mathbf{u}$), thus:

$$\mathbf{S}(t) = \frac{\partial \mathbf{x}(t)}{\partial \mathbf{u}} = \frac{\partial \mathbf{x}(t)}{\partial \mathbf{p}}\frac{\partial \mathbf{p}}{\partial \mathbf{u}} = \frac{\partial \mathbf{x}(t)}{\partial \mathbf{p}}\mathbf{A} \tag{18}$$

leading to:

$$\mathbf{P}_c(t) = \begin{pmatrix} \mathbf{\Phi}(t,t_0) & \frac{\partial \mathbf{x}(t)}{\partial \mathbf{p}}\mathbf{A} \\ \mathbf{0} & \mathbf{I} \end{pmatrix} \begin{pmatrix} \mathbf{P}_c & \mathbf{0} \\ \mathbf{0} & \mathbf{C} \end{pmatrix} \mathbf{\Psi}(t,t_0)^T \tag{19}$$

with

$$\mathbf{C} = \begin{pmatrix} r_0 & \cdots & \cdots & 0 \\ \vdots & \sigma_u^2(1) & & \vdots \\ \vdots & & \ddots & \vdots \\ 0 & \cdots & \cdots & \sigma_u^2(n) \end{pmatrix}, \in \mathbb{R}^{n+1 \times n+1} \tag{20}$$

Where it is important to notice that the first element of the noise sequence is drawn from a Normal distribution whose variance is the power of the noise. Undoubtedly, this formulation suffers from the curse of dimensionality. As the number of stochastic parameters increase, the matrices operations can become difficult to handle efficiently with simple matrix products. This topic is discussed further in this work as a trade-off between computational efficiency and accuracy.

2.4. From single to multiple parameters

According to the previously defined AR(1) model for the parameters, any propagation or determination arc could contain a large number of parameters. Thus, the nominal sensitivity matrix would contain thousands of parameters, being un-affordable to compute by soving the variational equations. This subsection describes how to exploit the properties of the variational equations to derive the multiple-parameters sensitivity matrix from the single parameter case.

Let us focus, for the sake of clarity, in a single uncertain parameter such as the atmospheric density error. Our objective now is to analyze the impact on covariance propagation of such parameter, but instead of being defined as a single, constant parameter during the complete arc of analysis, is now subdivided in many different parameters applicable at different epochs. This is, instead of assuming that a single value of the aerodynamic model error is applied to the whole arc, we define different subarcs in which different realizations of the uncertain parameter are considered. A diagram of this concept is shown in Figure 1, showing the different parameters $\mathbf{p_i}$ and their start and end times of application. Parameter $\mathbf{p_c}$ represents the previous unique parameter applied to the complete time arc.

First of all, the system dynamics are defined as

$$\frac{\partial \mathbf{x}}{\partial t} = \mathbf{f}(t, \mathbf{x}, \mathbf{p}); \quad \mathbf{x}(t_0) = \mathbf{x_0}. \tag{21}$$

The state transition matrix and sensitivity matrix are defined, respectively, as

$$\mathbf{\Phi} = \frac{\partial \mathbf{x}}{\partial \mathbf{x_0}} \tag{22}$$

$$\mathbf{S} = \frac{\partial \mathbf{x}}{\partial \mathbf{p}} \tag{23}$$

The variational equations are of the form [16]:

$$\frac{\partial \mathbf{\Phi}}{\partial t} = \frac{\partial \mathbf{f}}{\partial \mathbf{x}}\mathbf{\Phi}; \;\; \mathbf{\Phi}|_{t_0} = \mathbf{I} \tag{24}$$

$$\frac{\partial \mathbf{S}}{\partial t} = \frac{\partial \mathbf{f}}{\partial \mathbf{x}}\mathbf{S} + \frac{\partial \mathbf{f}}{\partial \mathbf{p}}; \;\; \mathbf{S}|_{t_0} = \mathbf{0} \tag{25}$$

Now, in order to separate this sensitivity matrix in the contribution of many parameters applicable in different time intervals, we define the individual sensitivity matrices of the parameters as

$$\mathbf{S_i}(t) = \frac{\partial \mathbf{x}(t)}{\partial p_i} \tag{26}$$

Which still has to fulfill

$$\frac{\partial \mathbf{S_i}}{\partial t} = \frac{\partial \mathbf{f}}{\partial \mathbf{x}}\mathbf{S_i} + \frac{\partial \mathbf{f}}{\partial p_i}; \quad \text{for } t_{pi} < t < t_{pi+1} \tag{27}$$

with

$$\mathbf{S_i}|_{t_p i} = \mathbf{0} \tag{28}$$

Where t_{pi} and t_{pi+1} correspond to the start and end epochs of application of the parameter, respectively (see Figure 1). The properties of the variational equations allow to relate sensitivity matrices resulting from the same model, with the only difference being the initial conditions. Therefore, the partial derivatives of the i^{th} parameter as a function of the overall partials of the constant, global parameter, is

$$\frac{\partial \mathbf{x}(t)}{\partial \mathbf{p_i}} = \frac{\partial \mathbf{x}(t)}{\partial \mathbf{p_c}} - \frac{\partial \mathbf{x}(t)}{\partial \mathbf{x}(t_{pi})}\frac{\partial \mathbf{x}(t_{pi})}{\partial \mathbf{p_c}} \quad \text{for } t_{pi} < t < t_{pi+1} \tag{29}$$

Where $\frac{\partial \mathbf{x}(t)}{\partial \mathbf{x}(t_{pi})} = \frac{\partial \mathbf{x}(t)}{\partial \mathbf{x_0}}\left(\frac{\partial \mathbf{x}(t_p i)}{\partial \mathbf{x_0}(t_{pi})}\right)^{-1}$. After the end epoch of the parameter (t_{pi+1}), its contribution to the state evolution is obtained through the state transition matrix starting at the end epoch, since beyond t_{pi+1} the parameter is no longer active, and thus $\left.\frac{\partial \mathbf{f}(t)}{\partial p_i}\right|_{t>t_{pi+1}} = 0$. This leads to:

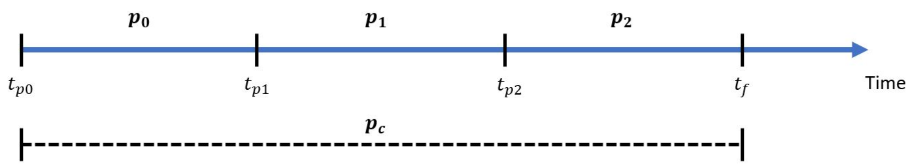

Figure 1: Parameters application timeline

$$\frac{\partial \mathbf{x}(t)}{\partial \mathbf{p_i}} = \frac{\partial \mathbf{x}(t)}{\partial \mathbf{x}(t_{pi+1})}\left(\mathbf{S_i}(t_{pi+1})\right) = \\ = \frac{\partial \mathbf{x}(t)}{\partial \mathbf{x}(t_{pi+1})}\left(\frac{\partial \mathbf{x}(t_{pi+1})}{\partial \mathbf{p_0}} - \frac{\partial \mathbf{x}(t_{pi+1})}{\partial \mathbf{x}(t_{pi})}\frac{\partial \mathbf{x}(t_{pi})}{\partial \mathbf{p_i}}\right) \\ \text{for } t > t_{pi+1} \tag{30}$$

Before the start epoch of the parameter (t_{pi}), the impact of the parameter is null: $\mathbf{S_i}(t_{pi+1})|_{t<t_{pi}} = 0$.

With this formulation, the sensitivity matrix for all the stochastic parameters affecting the noise sequence can be computed from a single-parameter sensitivity matrix, and then, the correlation is included via matrix $\mathbf{A}$ for the linear covariance propagation. It is relevant to highlight that all previously described steps for the LSP covariance propagation method are applicable to any kind of uncertain parameter that can be modelled with the AR(1) stochastic model sequence. This includes relevant and widely analysed parameters such as the solar radiation pressure coefficient or the errors in manoeuvre thrust magnitude and direction.

2.5. Limiting case: extremely high correlation

To further understanding of the proposed LSP method, the case of extremely high correlation is analysed in depth here. As previously described in Section 2.2, highly correlated noise ($\tau_\alpha \approx \infty$) will cause $a(n) \approx 1$ and $u(n) \approx 0$, thus ending up with a constant noise sequence. In such a case, the previously described LSP formulation should be equivalent to the original constant parameter covariance propagation. Assuming constant noise timestep and power noise, matrices $\mathbf{C}$ and $\mathbf{A}$ become

$$\mathbf{C} = \begin{pmatrix} r_0 & \cdots & \cdots & 0 \\ \vdots & 0 & & \vdots \\ \vdots & & \ddots & \vdots \\ 0 & \cdots & \cdots & 0(n) \end{pmatrix}, \in \mathbb{R}^{n+1\times n+1} \tag{31}$$

$$\mathbf{A} = \begin{pmatrix} 1 & \cdots & 0 \\ \vdots & \ddots & \vdots \\ 1 & \cdots & 1 \end{pmatrix} \in \mathbb{R}^{n+1\times n+1}, \tag{32}$$

If we focus only on the contribution of the sensitivity matrix to the covariance propagation, we have

$$\mathbf{P}_s(t) = \mathbf{S}(t)\cdot\mathbf{C}\cdot\mathbf{S}(t)^T = \left(\frac{\partial \mathbf{x}(t)}{\partial \mathbf{p}}\mathbf{A}\right)\mathbf{C}\cdot\mathbf{S}(t)^T \tag{33}$$

Due to the characteristics of $\mathbf{C}$ in this constant case, only the first column of matrix $\mathbf{A}$ is retained, which leads to

$$\mathbf{P}_s(t) = \begin{pmatrix} \sum \frac{\partial \mathbf{x_1}(t)}{\partial \mathbf{pn}} \\ \vdots \\ \sum \frac{\partial \mathbf{x_6}(t)}{\partial \mathbf{pn}} \end{pmatrix} \cdot r_0 \cdot \begin{pmatrix} \sum \frac{\partial \mathbf{x_1}(t)}{\partial \mathbf{pn}} \\ \vdots \\ \sum \frac{\partial \mathbf{x_6}(t)}{\partial \mathbf{pn}} \end{pmatrix}^T \tag{34}$$

And, due to Equation 29, $\sum_{i=1}^{N} \frac{\partial \mathbf{x_i}(t)}{\partial \mathbf{pn}} = \frac{\partial \mathbf{x_i}(t)}{\partial \mathbf{p0}}$, recovering the same equations as in the single parameter linear covariance propagation.

2.6. Monte Carlo covariance propagation

Monte Carlo methods are widely used for uncertainty propagation, and could be classified as non-linear non-Gaussian probabilistic UP methods. They are based on the selection of a set of independent and randomly distributed samples, and then those samples are propagated through the non-linear process [19]. They are suitable for the representation of any PDF and are not complex to implement. However, depending on the application and the target PDF, a high number of samples may be required to ensure the convergence of the method to the real solution, being computationally expensive. The MC method for the propagation of the covariance is summarised as follows.

Let $\widehat{\boldsymbol{x}}_n$ be the initial state, with its associated covariance $\boldsymbol{C}_n$ representing the PDF of the state. From these initial conditions, a number N_{MC} of independent and randomly distributed samples are generated following a multivariate normal distribution as follows

$$\boldsymbol{x}_n^i \sim \boldsymbol{N}\left(\widehat{\boldsymbol{x}}_n, \boldsymbol{C}_n\right), \quad i = 1, \ldots, N_{MC}. \tag{35}$$

Each of these samples is propagated forward in time according to the given dynamics of the system as

$$\boldsymbol{x}_{n+1}^i = \boldsymbol{f}\left(\boldsymbol{t}, \boldsymbol{x}_n^i\right). \tag{36}$$

In this work, the dynamics of the system for the MC propagation include the same stochastic model of the atmosphere density for validation purposes. Finally, the state and covariance matrix after the propagation can be estimated as follows, where only the first and second moment of the final PDF are retained:

$$\widehat{\boldsymbol{x}}_{n+1} = \frac{1}{N} \sum_{i=1}^{N} \left[\boldsymbol{x}_{n+1}^{i} \right] \tag{37}$$

$$\boldsymbol{C}_{n+1} = \frac{1}{N} \sum_{i=1}^{N} \boldsymbol{x}_{n+1}^{i} \left(\boldsymbol{x}_{n+1}^{i} \right)^{T} - \widehat{\boldsymbol{x}}_{n+1} \widehat{\boldsymbol{x}}_{n+1}^{T} \tag{38}$$

3. VALIDATION

This section, the procedure for the validation of the LSP covariance propagation method is detailed first, providing a description of the test cases, the RSO characteristics and the dynamic model. Then, the results of the validation are presented and discussed.

3.1. Validation procedure

As previously mentioned, the proposed method is validated via Monte Carlo simulations using stochastic dynamics for two different LEO scenarios. The characteristics of the test cases and their corresponding RSO are summarized in Table 1:

Table 1: Test cases summary

	RSO1	**RSO2**
Altitude [km]	800	450
A/M ratio $[m2/kg]$	0.1	0.02
Semi-major axis	7181.994 km	6815.219 km
Eccentricity	1.387	1.612
Inclination	98.557º	87.411º
RAAN	314.523º	138.472º
Argument of pericenter	77.836º	61.090º
True anomaly	70.547º	160.057º
Drag coefficient	2.84	0.485
Reference epoch	05/09/2018 17:21:10.411 UTC	12/09/2017 14:38:22.100 UTC
MC $\sigma_{atm}[kg/m^3]$	5.0e-16	5.86e-14
Samples	200	200

The two test cases correspond to LEO objects with a circular orbits at an altitude of approximately 450 km of altitude, where the drag force becomes one of the most relevant perturbations, and at 800 km, where impact of the drag acceleration is lower. The chosen absolute uncertainty of the atmosphere (σ_{atm}) is different in the two cases in order to adapt to the variation in mean density at such altitudes, taken from the atmospheric uncertainty results of [6][1]. The dynamic model used in the high-fidelity propagator for the Monte Carlo simulations can be seen in Table 2.

For each correlation time scale under analysis, an independent Monte Carlo simulation is carried out, whose steps are summarized as:

1. 200 samples are generated from the initial state and covariance of the RSO
2. Each sample is propagated 7 days, with SDE dynamics that include the stochastic drag model defined in Section 2.2 and an integration time-step of 10 seconds
3. For each propagation, the corresponding noise power to the RSO is applied (σ_{atm}), as well as the selected correlation time scale
4. The covariance at each propagation epoch is reconstructed following the process described in Section 2.6

Please refer to [6] for more details about the Monte Carlo simulations with SDE dynamics. Regarding the initial covariance, only position and velocity covariance have been considered as initial PDF, not including any drag a-priori covariance. The reason is that the purpose of the methodology is to represent the drag uncertainty by means of the stochastic density model, instead of sampling an a-priori drag covariance. The initial covariance matrices for both RSO can be found in [6]. It is worth mentioning that, as discussed in [6], the differences between 200 and 2000 samples Monte Carlo benchmark were sufficiently small so that the MC results with 200 samples can be considered as reference values for the validation. Further testing with an increased amount of samples are left for future works.

In the case of the LSP covariance propagation, a single 7 days propagation of each RSO is carried out, with the same dynamic model, and no stochastic component in the drag acceleration. This would be equivalent to any orbit propagation in nominal operations. From this process, it is obtained the propagated ephemeris, the state transition matrix ($\boldsymbol{\Phi}(t, t_0)$) and the partial derivatives with respect to the global parameter ($\frac{\partial \mathbf{x}(t)}{\partial \mathbf{p_c}}$) described in Section 2.4. Having such information, the LSP covariance propagation methodology requires the initial state and covariance of the RSO, a power of the noise in relative terms σ_{atm}/ρ, the time scale of analysis and a desired number of stochastic parameters to include in the propagation arc (N of Equation 17).

Table 2: Dynamic model

Reference frame	J2000 ECI
Gravity field	32x32
Third body perturbations	Sun & Moon
Earth geodetic surface	ERS-1
Polar motion and UT1	IERS C04 08
Earth pole model	IERS 2010 conventions
Earth precession/ nutation	IERS 2010 conventions
Atmospheric model	NLRMSISE-00
Solar radiation pressure	Not considered
Propagation step	10 seconds

3.2. Validation results

The following results focus on the along-track standard deviation (σ_T) of the propagated covariance in the TNW local reference frame. Being aligned with the direction of the velocity, this direction is expected to accumulate most of the errors and uncertainty associated to the drag force. Figure 2 below shows the evolution of σ_T with propagation time, for some examples of correlation time scales, comparing the results obtained with the LSP covariance propagation (dashed lines) against the Monte Carlo results (continuous lines).

The relative sigma $\overline{\sigma}_{atm}$ applied in each case is also showed in Figure 2. It is relevant to mention that the current implementation of the LSP method expected a constant power noise in relative terms ($\overline{\sigma}_{atm}$). However, the SDE dynamic of the Monte Carlo apply a constant absolute σ_{atm}, which does not yield a constant $\overline{\sigma}_{atm}$ since the NRLMSISE-00 model is applied during the propagation, with varying density depending on the epoch and location of the RSO. Therefore, the $\overline{\sigma}_{atm}$ values applied for the LSP covariance propagation are computed by dividing the σ_{atm} values of Table 1 by the mean density along the propagation period.

Figure 2a depicts the time evolution of the along-track standard deviation for different correlation time scales, comparing the LSP with the Monte Carlo benchmark. It has been chosen a parameter time step of 5 minutes, which represents the interval of time at which each parameter is acting. This is, the lower the parameter time step, the larger the amount of stochastic parameters included in the LSP analysis, and vice-versa.

As will be commented in further detail in Section 4, the along-track standard deviation grows faster in time with increasing the amount of correlation, reaching convergence to a maximum for time-scales greater than the propagation period. As expected, the growth is larger at lower altitudes, due to higher density. In addition to this, Figure 2a shows that the LSP covariance propagation method follows closely the Monte Carlo results. However, in the RSO2 case for a lower altitude, both methods match except at very small correlation scales, equivalent to purely Gaussian noise. The reason for this different lies on the 5 minutes time step of the parameters, as explained next.

On the one side, the purely Gaussian case is expected to provide the smallest covariance growth since, if the acceleration is perturbed randomly, with a zero-mean constant variance, and at a high frequency (10 seconds of integration step in MC), the perturbations are expected to approximately cancel out during the propagation. It is important to remark that the perturbations are applied to the acceleration directly, and not assumed as a Gaussian step noise like a Wiener noise. On the other side, the frequency of the perturbation that the LSP method is able to represent depends on the number of stochastic parameters, or analogously, on the parameter time step. Though this is observed not to be relevant for high time correlation or high altitudes, this issue becomes noticeable in the lower altitude case, where the drag force is becoming dominant, not allowing to cancel completely the purely Gaussian noise by including a parameter each 5 minutes.

Figure 3 represents the relative σ_T error with respect to MC Gaussian noise, comparing 1 and 5 minutes of parameters time step. It can be seen how the error is largely reduced when decreasing the step. However, the 1 minute step still results in more than 100% of error, with clear room for improvement. Both methods would converge by reducing the step further, but a trade-off must be made between accuracy and computational efficiency. It is also seen that the accuracy at larger correlations is less affected by the parameter step.

To assess in more detail the achieved accuracy with the LSP covariance propagation, Figure 4 depicts the contour of the relative error as compared to the Monte Carlo simulations, for a wide range of correlation time scales and as a function of the propagation time. The y-axis represents the correlation time scale, but normalized with the period of the orbits, a magnitude of relevance for correlation analysis. 5 minutes step for the parameters is maintained in Figure 4.

In the case of the high altitude RSO (Figure 4a), the error is kept below a 10%, finding the maximum error at correlation scales between the orbital period (around 1.5 hours) and 10 orbital periods. Firstly, the correlation impact on the covariance growth becomes noticeable upon reaching correlation scales of the order of the orbital period, converging to the upper limit of constant correlation. Therefore, the errors are expected to be larger in such areas. However, the reason for the observed errors was found to be the differences in the relative atmospheric density uncertainty of both methods, the LSP and the MC simulations, as discussed previously. Though the LSP applies an averaged $\overline{\sigma}_{atm}$, when large periods of propagation do not match the effective uncertainty in the MC simulations, both methodologies diverge slightly.

In Figure 4b, the purely Gaussian correlation scale lower bound has been removed from the graph, for proper visualization of the accuracy at the rest of the correlation spectrum. In this case, analogous conclusions to the high altitude RSO case can be extracted. The error is kept below a 16% and, though the error is centered as in the previous case around 1 and 10 orbital periods, it is more

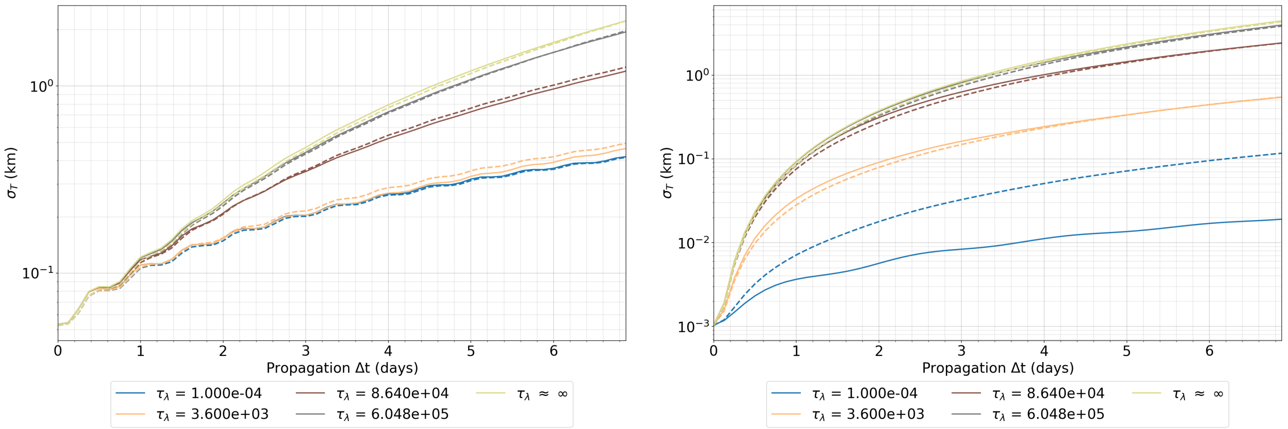

(a) RSO1, $\overline{\sigma}_{atm} = 0.219$

(b) RSO2, $\overline{\sigma}_{atm} = 0.131$

Figure 2: σ_T time evolution for different time scales $\tau_\lambda(s)$. Continuous lines represent the results from the MC simulation. Dashed lines represent the LSP covariance propagation results, for the same $\tau_\lambda(s)$. 5 minutes of parameter time step

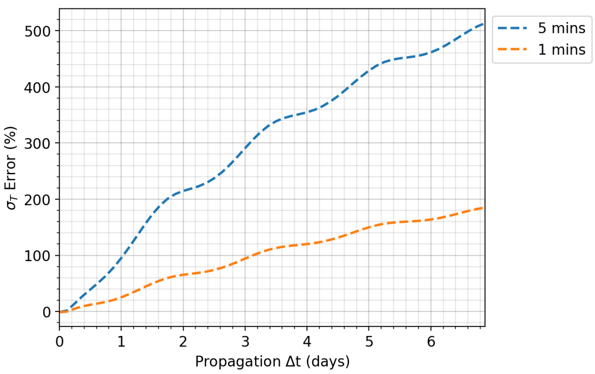

Figure 3: RSO2, relative error for Gaussian correlation between LSP method and MC simulations for different LSP data time-steps

spread across the correlation scales. Again, the reason found was the differences in applied $\overline{\sigma}_{atm}$ in the MC simulations, which in this case were further from the mean at the beginning of the propagation, as seen in 4b.

Contour plots of the error results applying a parameter step of 1 minute have been omitted since the accuracy was, in general, the same as in the cases presented here except at low altitudes and very low correlation. For further validation of the LSP method, new MC simulations that enforce a constant $\overline{\sigma}_{atm}$ must be carried out as future work. Nonetheless, it can be highlighted that levels of accuracy below 10 and 16% are achieved using a parameter step of 5 minutes, compared against MC simulations applying high-accuracy atmospheric density models, which is considered a promising result.

4. RESULTS

After assessing the accuracy of the LSP method through validation in Section 3, this section provides further discussion regarding the performance of the method. The focus is placed on the covariance growth obtained as a function of the correlation and the efficiency of the LSP method.

Figure 5 depicts the time evolution of the along-track standard deviation for both RSOs, using the LSP methodology again with a parameter step of 5 minutes. As expected, the growth is larger for the lower altitude RSO due to the higher mean atmospheric density at 450 km of altitude, reaching more than 3 km after the correlation time scale surpasses 10 times the orbital period. In both cases, the most relevant covariance growth is observed for time scales greater than 10 orbital periods, roughly half a day. Afterwards, the covariance grows more rapidly until reaching convergence after the correlation time scales are beyond half the propagation period (3.5 days).

In Appendix A, 2D dispersion plots of the Monte Carlo samples are shown (Figures 7, 8), where the LSP method covariance is checked to be representative of the uncertainty for the RSOs and propagation arcs considered. The purpose of this kind of analysis is to control that the system has not deviated too far from the linear and Gaussian assumptions, so that the covariance is still a proper representation of the uncertainty of the state. These results are in line with previous studies [6], where more RSO cases are analysed for SDE dynamics.

Figure 6 represents again the along-track covariance growth for RSO1 case, but normalizing the covariance with the final covariance results for each correlation scale. It is appreciated that for purely Gaussian (no-correlation), or reduced time scales, the covariance grows linearly with time. However, an exponential growth of the covariance is observed for increasing correlation, with

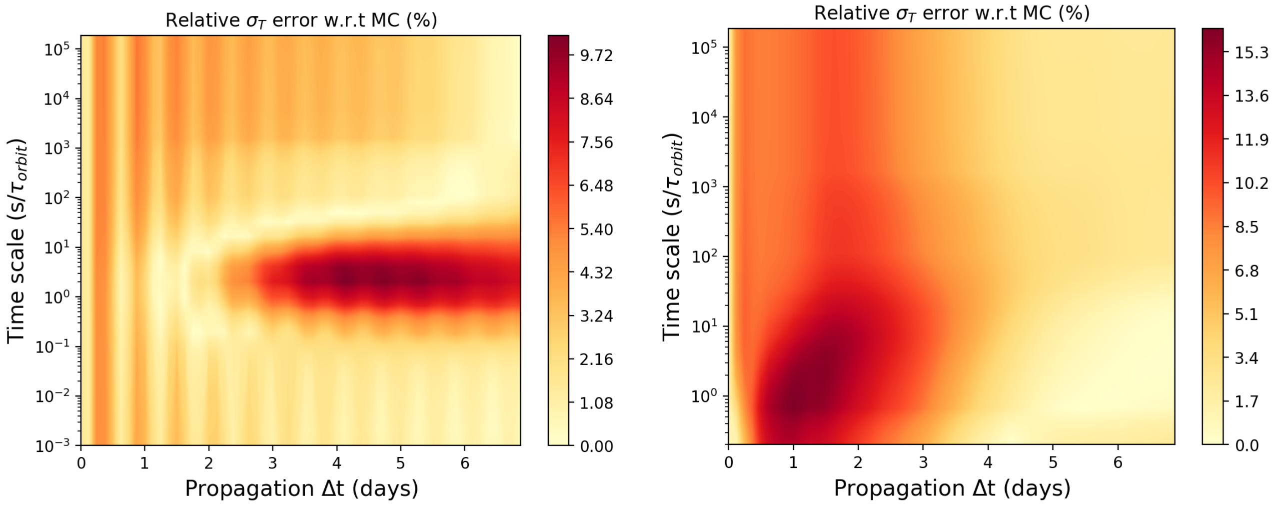

(a) RSO1, $\overline{\sigma}_{atm} = 0.219$

(b) RSO2, $\overline{\sigma}_{atm} = 0.131$

Figure 4: σ_T relative error contour, for an LSP parameter time step of 5 mins

an exponential slope proportional to the correlation time scale.

Finally, a relevant aspect to analyse is the computational time achieved with the proposed methodology. Table 3 shows averaged CPU times of execution for the LSP propagation method and the Monte Carlo benchmark. The LSP results are averaged over 70 executions with different time-scales, both RSOs, and correspond to a single kernel execution (Intel(R) Core(TM) i7-8665U CPU @ 1.90GHz 2.11 GHz). Monte Carlo simulation times are also shown with 6 cores parallelisation, with a || symbol.

It is shown that 78% of performance can be gained if using the LSP method with a 5 minutes parameter step, as compared to the 200 samples MC with parallelisation. This performance improvement values are to be taken with caution, since the parallelisation viability for the LSP method is yet to be studied, and Monte Carlo methods could be executed with more kernels, if available. As expected, with increasing the numer of parameters, the efficiency of the methodology is deteriorated significantly, as seen in the 1 minute parameter step results of Table 3. However, it is relevant to notice that the execution performances showed in Table 3 for the LSP method correspond to the computation of all covariance matrices at each propagation step, which also increases the computational cost. If only few epochs of the covariance are of interest, the LSP computational costs of Table 3 are reduced.

Therefore, a remarkable efficiency improvement can be achieved with the LSP methodology, having an error lower than 15% even at a low altitude case. Further assessment of the LSP performance and accuracy are planned lines of study. For parameter time steps of around 10 seconds (similar steps to the integration step), the LSP method time performance is decreased substantially, due to the curse of dimensionality as the number of stochastic parameters increase. It has been showed that lower time steps are only required for accuracy at very small correlation and low altitudes. Therefore, the methodology for increasing the number of parameters, specifically for very low correlation, is a line of improvement.

Table 3: CPU time comparison between LSP covariance propagation and Monte Carlo.

Method	**Average CPU time [h]**
MC 2000 samples	7.33
MC 200 samples	1.04
MC 2000 samples ||	1.22
MC 200 samples ||	0.17
LSP (5 min)	0.04
LSP (1 min)	0.26

5. CONCLUSIONS AND FUTURE WORK

In this work, the LSP covariance propagation methodology has been described. It exploits the linear propagation theory and the properties of the variational equations, allowing to analyse the effect on the covariance of time-correlated errors of stochastic dynamic models. The atmospheric density of an orbiting RSO has been modelled with an AR(1) function for the stochastic drag model, and it has been described how to include the effect of multiple stochastic parameters in the covariance evolution.

The LSP method has been validated against Monte Carlo simulations that apply an analogous stochastic drag model on their equations of motion, for 2 different objects at high and low LEO altitudes. The evolution of the along-track covariance during a 7 days propagation

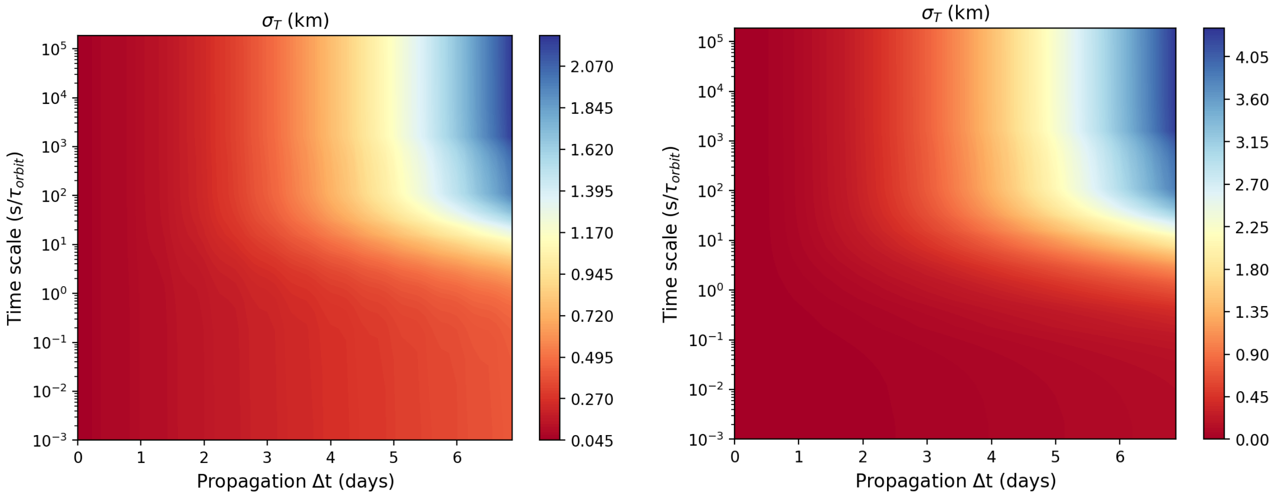

(a) RSO1, $\overline{\sigma}_{atm} = 0.219$ (b) RSO2, $\overline{\sigma}_{atm} = 0.131$

Figure 5: LSP covariance propagation results for σ_T as a function of time correlation and propagation time. LSP parameter step of 5 minutes

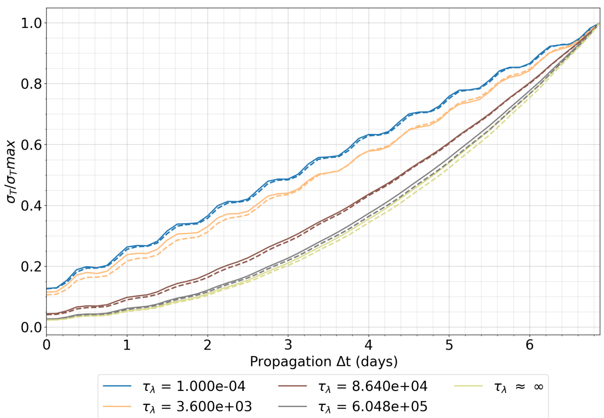

Figure 6: RSO1, growth of relative σ_T for different correlation time scales. Continuous lines represent the results from the MC simulation. Dashed lines represent the LSP covariance propagation results, for the same $\tau_\lambda(s)$. LSP parameter step of 5 minutes. $\overline{\sigma}_{atm} = 0.219$

period has been analysed for a wide range of correlation times scales, which represent the strength of the correlation. It is shown that an error below 10% and 15% is achieved for an 800 km and 450 km altitude RSOs, respectively, and as compared to the Monte Carlo benchmark with stochastic dynamics and complete atmospheric density model. For the low altitude RSO, very low time scales of the correlation (almost no-correlated noise, close to pure Gaussian noise) result in large relative error. The reason is that the frequency of the perturbations for the LSP method is limited by the amount of parameters that are modelled with their parameter application time step, which becomes relevant for the required accuracy at very low correlation. Due to the curse of dimensionality of the method as a function of the amount of perturbation parameters, further reductions of the parameter step become impractical in terms of CPU performance with the current methodology formulation, which is a future line of improvement. Furthermore, the LSP method has been shown to have a remarkable potential for time efficiency. It has shown up to a 78% improvement in computational cost while having around a 10-15% error.

Nonetheless, the results presented here correspond to the first prototype and tests of the LSP covariance propagation method, and there is still a wide room for improvement and further analysis. Firstly, the main source of the errors with respect to the Monte Carlo benchmark are due to a difference in the relative uncertainty of the atmosphere applied in both methods, caused by small implementation differences. Thus, further tests enforcing a purely constant relative uncertainty of the atmosphere must be conducted to assess the maximum accuracy achievable with LSP method. However, having between a 10-15% of error as compared with a realistic density simulation is a satisfactory result for these preliminary tests. Moreover, due to the observed accuracy loss at low correlation and low altitudes, the software efficiency at such regions must be upgraded in order to assimilate a higher number of stochastic parameters with enough computational time performance. Also, further tests in more varied scenarios and RSOs characteristics are required. Finally, it is worth reminding that the proposed LSP method is compatible with other uncertain parameters in the space environment, such as the SRP or manoeuvre uncertainty. Thus, the performance and suitability of the LSP covariance propagation method for more uncertain parameters is to be assessed in future work.

ACKNOWLEDGMENTS

This project has received funding from the "Comunidad de Madrid" under "Ayudas destinadas a la realización de doctorados industriales" program (project IND2020/TIC-17539).

REFERENCES

1. Aguado JB, Santiago JL, Yela AL, et al (2021) Uncertainty propagation meeting space debris needs. In: 8th European Conference on Space Debris, URL https://conference.sdo.esoc.esa.int/proceedings/sdc8/paper/253/SDC8-paper253.pdf
2. Alspach D, Sorenson H (1972) Nonlinear bayesian estimation using gaussian sum approximations. IEEE Transactions on Automatic Control 17(4):439–448. https://doi.org/10.1109/TAC.1972.1100034
3. Armellin R, Di Lizia F, Bernelli Zazzera F, et al (2009) Apophis encounter 2029: differential algebra and taylor model approaches. In: 1st IAA Planetary Defence Conference
4. Armellin R, Di Lizia P, Bernelli Zazzera F, et al (2010) Nonlinear mapping of uncertainties: a differential algebraic approach. In: 4th International Conference on Astrodynamics Tools and Techniques (ICATT), 2010-04-29 - 2010-04-30, Madrid, Spain
5. Brockwell PJ, Davis RA (2016) Introduction to Time Series and Forecasting. Springer
6. Cano A, Gago P, Pastor A, et al (2022) Atmospheric correlation impact in uncertainty propagation. In: 3rdInternational Conference on Space Situational Awareness(ICSSA), ICSSA, AA-ICSSA-22-0007
7. Cools R (1992) A Survey of Methods for Constructing Cubature Formulae, Springer Netherlands, Dordrecht, pp 1–24. https://doi.org/10.1007/978-94-011-2646-5_1, URL https://doi.org/10.1007/978-94-011-2646-5_1
8. DeMars KJ, Bishop RH, Jah MK (2013) An entropy-based approach for uncertainty propagation of nonlinear dynamical systems. Journal of Guidance, Control, and Dynamics 36(4):1047–1057. https://doi.org/10.2514/1.58987
9. Emmert J, Warren H, Segerman A, et al (2017) Propagation of atmospheric density errors to satellite orbits. Advances in Space Research 59(1):147–165. https://doi.org/10.1016/j.asr.2016.07.036
10. Hoffman FO, Hammonds JS (1994) Propagation of uncertainty in risk assessments: the need to distinguish between uncertainty due to lack of knowledge and uncertainty due to variability. Risk Analysis pp 14(5): 707–712
11. Jones BA, Doostan A, Born GH (2013) Nonlinear propagation of orbit uncertainty using non-intrusive polynomial chaos. Journal of Guidance, Control, and Dynamics 36(2):430–444. https://doi.org/10.2514/1.57599
12. Julier S, Uhlmann J (2004) Unscented filtering and nonlinear estimation. Proceedings of the IEEE 92(3):401–422. https://doi.org/10.1109/jproc.2003.823141
13. zhong Luo Y, Yang Z (2017) A review of uncertainty propagation in orbital mechanics. Progress in Aerospace Sciences 89:23–39. https://doi.org/10.1016/j.paerosci.2016.12.002
14. Mashiku AK, Garrison J, Carpenter JR (2012) Statistical orbit determination using the particle filter for incorporating non-gaussian uncertainties. In: 2012 AIAA/AAS Astrodynamics Specialist Conference, Minneapolis
15. McCabe JS, DeMars. KJ (2014) Particle filter methods for space object tracking. In: AIAA/AAS Astrodynamics Specialist Conference. American Institute of Aeronautics and Astronautics (AIAA), San Diego, CA
16. Montenbruck O, Gill E (2000) Satellite Orbits: Models, Methods and Applications. Springer-Verlag Berlin Heidelberg, Berlin, https://doi.org/10.1007/978-3-642-58351-3
17. Park RS, Scheeres DJ (2006) Nonlinear mapping of gaussian statistics: Theory and applications to spacecraft trajectory design. Journal of Guidance, Control, and Dynamics 29(6):1367–1375. https://doi.org/10.2514/1.20177, URL https://doi.org/10.2514/1.20177, https://arxiv.org/abs/https://doi.org/10.2514/1.20177
18. Poore AB, Aristoff JM, Horwood JT, et al (2016) Covariance and Uncertainty Realism in Space Surveillance and Tracking. Tech. rep., Numerica Corporation Fort Collins United States, URL https://apps.dtic.mil/docs/citations/AD1020892
19. Robert CP, Casella G (2004) Monte Carlo statistical methods. Springer
20. Sagnieres L, Sharf I (2017) Uncertainty characterization of atmospheric density models for orbit prediction of space debris. In: Proceedings of the 7th European Conference on Space Debris. ESA Space Debris Ofice, Darmstadt, Germany
21. Schiemenz F, Utzmann J, Kayal H (2019) Least squares orbit estimation including atmospheric density uncertainty consideration. Advances in Space Research 63(12):3916–3935. https://doi.org/10.1016/j.asr.2019.02.039
22. Tapley BD (1975) Orbit determination in the presence of unmodeled accelerations. Tech. rep., Air Force Office of Scientific Research
23. Tapley BD, Schutz BE, Born GH (2004) Statistical Orbit Determination. Elsevier Academic Press, San Diego, California

24. Vallado DA (1997) Fundamentals of Astrodynamics and Applications, forth edn. Space Technology Library, Springer and Microcosm Press, Hawthorne, CA
25. Vallado DA, Finkleman D (2014) A critical assessment of satellite drag and atmospheric density modeling. Acta Astronautica 95:141–165. https://doi.org/10.1016/j.actaastro.2013.10.005
26. Vittaldev V, Russell RP (2016) Space object collision probability using multidirectional gaussian mixture models. Journal of Guidance, Control, and Dynamics 39(9):2163–2169. https://doi.org/10.2514/1.g001610
27. Xiu D, Karniadakis G (2002) The wiener–askey polynomial chaos for stochastic differential equations. SIAM J Sci Comput 24:619–644. https://doi.org/10.1137/S1064827501387826

APPENDIX A

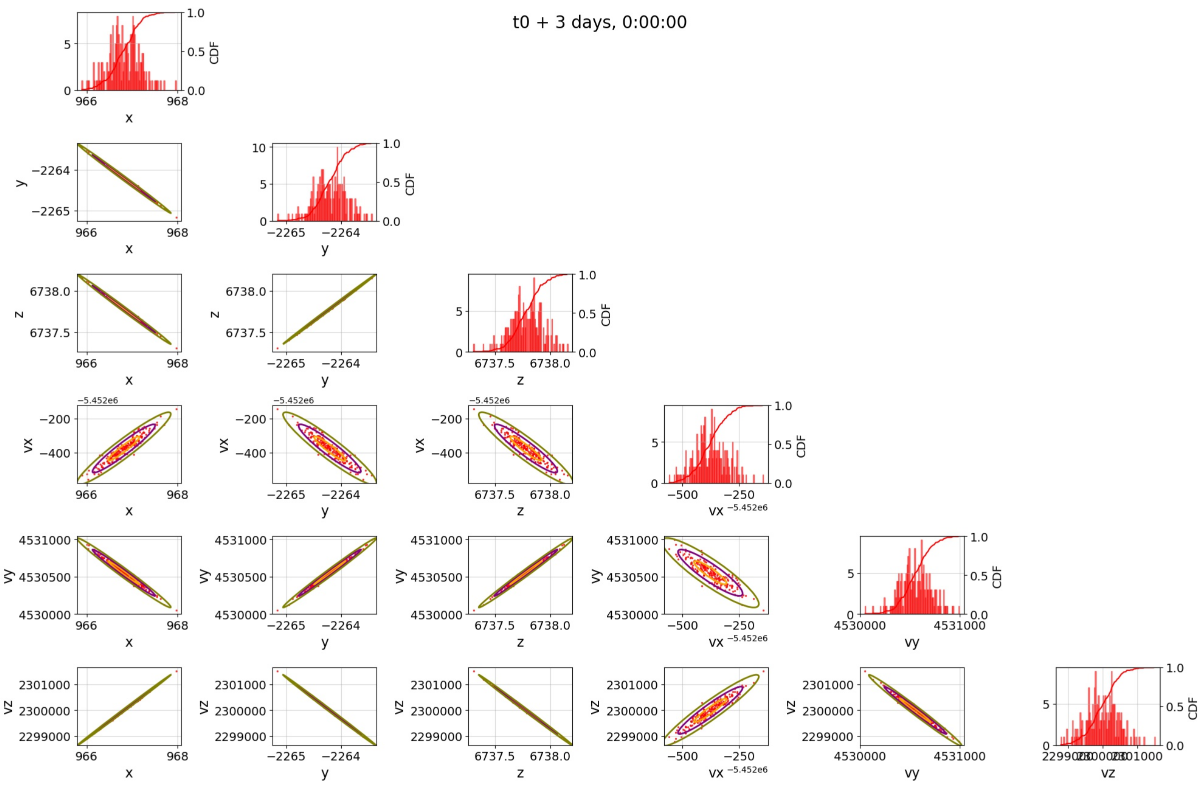

Figure 7: 2D Monte Carlo points distribution plots, for RSO1 after 3 days of propagation, applying a large time correlation. LSP sigma ellipsoids are overlapped (1,2,3 σ). The Monte Carlo points are clearly contained withing the 3σ ellipsoid for almost all points. LSP parameter step of 5 mins.

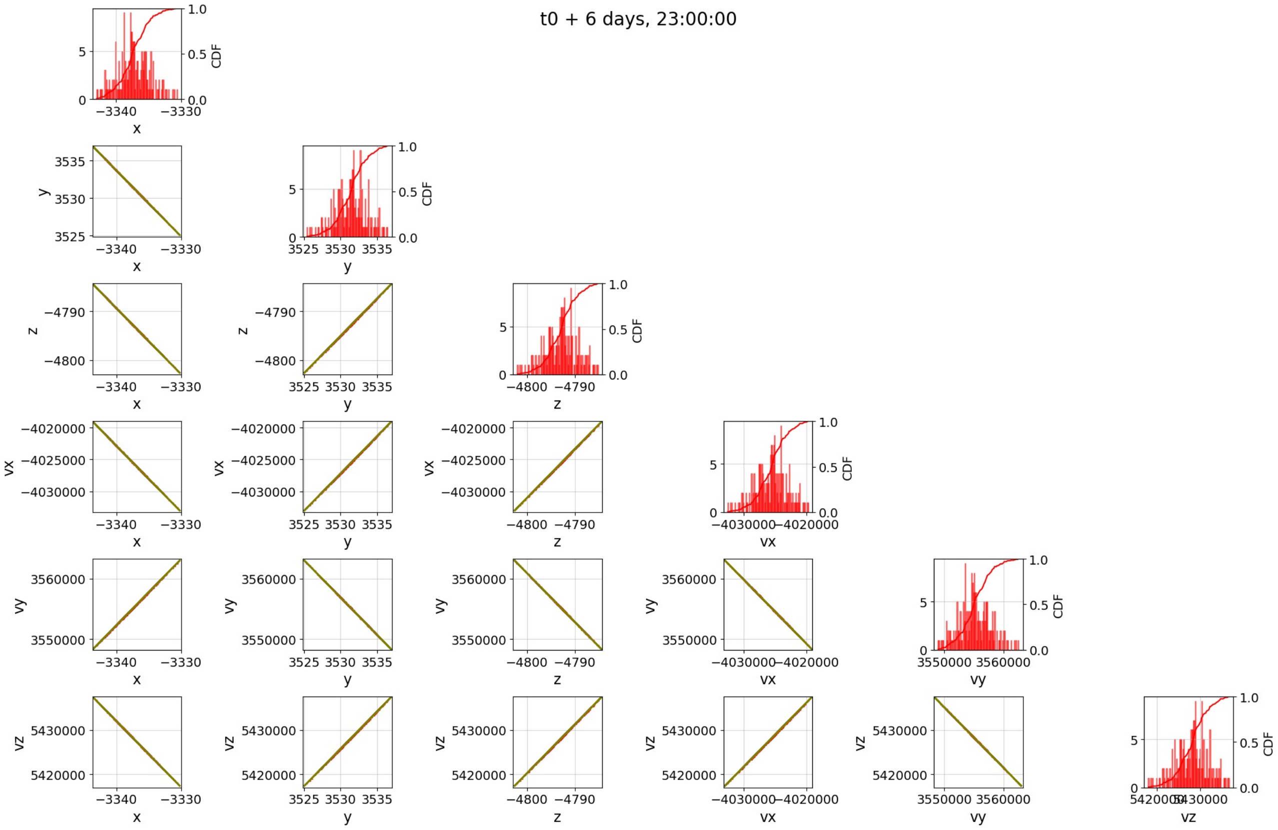

Figure 8: 2D Monte Carlo points distribution plots, for RSO2 after 6 days of propagation, applying a large time correlation. LSP sigma ellipsoids are overlapped (1,2,3 σ). LSP parameter step of 5 mins. Though stretched due to the large covariance growth, the MC points are still within the ellipsoid and the diagonal distributions are close to Gaussian. The so-called banana-shapes are not yet found.